

RSC Advances



This is an *Accepted Manuscript*, which has been through the Royal Society of Chemistry peer review process and has been accepted for publication.

Accepted Manuscripts are published online shortly after acceptance, before technical editing, formatting and proof reading. Using this free service, authors can make their results available to the community, in citable form, before we publish the edited article. This *Accepted Manuscript* will be replaced by the edited, formatted and paginated article as soon as this is available.

You can find more information about *Accepted Manuscripts* in the [Information for Authors](#).

Please note that technical editing may introduce minor changes to the text and/or graphics, which may alter content. The journal's standard [Terms & Conditions](#) and the [Ethical guidelines](#) still apply. In no event shall the Royal Society of Chemistry be held responsible for any errors or omissions in this *Accepted Manuscript* or any consequences arising from the use of any information it contains.

Intramolecular Charge Transfer Interactions and Molecular Order of Rod like Mesogens

M. Guruprasad Reddy,^a Nitin P. Lobo,^b E. Varathan,^c S. Easwaramoorthi,^c and T. Narasimhaswamy*^a

^a Polymer Laboratory, ^b Chemical Physics Laboratory and ^c Chemical Laboratory, CSIR-Central Leather Research Institute, Adyar, Chennai, India-600020.

*E-mail: tnsawamy99@hotmail.com

Abstract

A mesogenic 4-((4-(alkoxy)phenoxy)carbonyl)phenyl-4-(dimethylamino)benzoate series with terminal chain varying from C₂ to C₁₂ carbons (even number carbons only) are synthesised and their mesophase transitions are examined by hot-stage optical polarising microscopy as well as differential scanning calorimetry. Accordingly, enantiotropic nematic mesophase for all the homologs and an additional smectic A phase for C₁₂ homolog is observed. Powder X-ray diffraction studies confirm the interdigitated bilayer organization in smectic A phase for the C₁₂ homolog. It is remarkable that the mesogens under investigation only differ in the linking unit i.e. ester versus imine in contrast to recently reported mesogens, yet show large difference in certain properties. Accordingly, the crystal structure of C₄ homolog reveals triclinic lattice with P1 space group in which the molecules are packed in slipped co-facial configuration. Additionally, a detailed investigation of C₁₂ mesogen by UV-visible and fluorescence spectroscopy as well as computational methods unveils interesting features. The fluorescence spectrum of C₁₂ mesogen is observed at 366 nm with a shoulder at 433 nm and a large solvent polarity induced red-shift is noticed in contrast to structurally similar homolog examined recently. Further, the C₁₂ mesogen in solvents such as ethyl acetate, dichloromethane, chloroform, tetrahydrofuran, acetonitrile and dimethyl sulfoxide exhibited dual emission. Therefore, density functional theory and time dependent density functional theory calculations are utilized to get the insight. Besides variation in dihedral angle between rings B and C for C₁₂ mesogen, it is found that the highest occupied molecular orbital (HOMO) is localized on N, N-dimethylaminobenzene moiety while lowest unoccupied molecular

orbital (LUMO) is mostly concentrated on the phenyl benzoate unit. The Time dependent-density functional theory (TD-DFT) calculations disclose the orbitals involved in the dominant excited state electronic transitions and their corresponding energies together with oscillator strength. The high resolution 1D and 2D separated local field (SLF) solid state ^{13}C NMR investigation of C_{12} mesogen lead to the orientational order parameters of phenyl rings of the core in SmA_d phase. The temperature versus alignment induced chemical shifts reveals increase in chemical shifts with decrease in temperature in smectic A_d phase in concurrence with order parameter values. Thus, understanding the photophysical properties of mesogens with dimethylamino moieties would facilitate better design of molecules for application in organic light emitting diodes for polarized emission.

Keywords: Smectic a_d , Fluorescence, VT-XRD, ^{13}C - ^1H Dipolar couplings, Orientational order

1. Introduction

Thermotropic liquid crystals are an important class of molecular materials and their growing prominence is attributed to spontaneous response to external stimuli.¹ The supramolecular organization at molecular level and macroscopic flow of these materials lead to exciting and interesting mesophases with intricate morphologies.² Innumerable molecular designs for complex mesogens have been emerged in recent literature with a radical change in synthetic strategy.³ Despite these exciting developments, the fundamental interest on structure-mesophase correlation of rod-like (calamitic) mesogens is enduring since subtle change in the molecular structure, dramatic change in properties are regularly seen.⁴ Therefore, the rod-like molecules serve as standard mesogens for evaluating the role of different moieties such as the core, linking units as well as terminal chains. In this class of rod-like mesogens, for several reasons, core unit built with three phenyl rings are distinct. For example, the presence of three phenyl rings in the core ensures liquid crystallinity and by

judicious selection of linking units as well as terminal groups, polymesomorphism can be induced.⁵ It is well-known that attachment of lengthy alkoxy chains to the core in rod-like molecules favor smectic mesophases while shorter chains produce nematic phase.⁶ Additionally, the insertion of terminal polar groups like NO₂, CN not only favours smectic polymesomorphism but also ensure the re-entrant phenomena.^{7,8} Also, thermal stability of three ring core mesogens is reasonably high in contrast to two ring molecules due to conjugation of phenyl rings mediated by linking units which enhance the molecular anisotropic polarizability.⁵

Molecular materials with dimethylamino group have attracted considerable attention due to their fundamental importance in photo-induced intramolecular charge transfer and their applications in sunscreens.⁹ Of particular interest is on 4-dimethylaminobenzoates in which dimethylamino acts as a donor while the benzoate moiety as acceptor.¹⁰ As a result these molecular systems have been used as important model molecules in probing many aspects of excited intramolecular charge transfer state.¹¹ Further, the 4-(N, N-dimethylamino) benzoate based molecules are found to exhibit twisted intra molecular charge transfer interactions with dual fluorescence.¹² Despite many studies on dimethylamino based molecular systems, detailed investigations on mesogens with dimethylamino group are limited.¹³ Furthermore, the current emphasis on donor-acceptor based π -conjugated molecules for their applications in organic light emitting diodes as well as organic photo voltaics also augmented the curiosity on molecules with dimethylamino moiety.^{14,15} Recently, we reported mesogens consisting of three phenyl ring core with a terminal N, N-dimethylamino group which exhibited interesting photophysical properties in addition to enantiotropic mesophases.¹⁶ In this work, we report yet another series of mesogens built with ester linking groups since the imine linkage has less conformational flexibility and less hydrolytic stability than ester unit. The main motivation of the investigation is the

observation of contrasting photo physical properties as well as the molecular packing of the mesogens explored in this work as against the earlier series¹⁶ though the change in the molecular structure is subtle. Thus the work reports besides the crystal structure of C4 mesogen, the liquid crystalline properties of homologs by hot-stage polarizing microscopy (HOPM) and differential scanning calorimetry (DSC) as well as photo physical properties. Further, the variable temperature powder X-ray diffraction (VT-XRD) of one of C12 homolog revealed interdigitated bilayer smectic A phase (SmA_d) while the solid state ¹³C NMR studies offered orientational order parameters of the phenyl rings of the core unit in liquid crystalline phase.

2. Experimental Section

The synthesised mesogens are listed below with expanded names and codes:

- (a) 4-((4-(ethoxy)phenoxy)carbonyl)phenyl-4-(dimethylamino)benzoate {5(a)}: EPCPDB
- (b) 4-((4-(butoxy)phenoxy)carbonyl)phenyl-4-(dimethylamino)benzoate {5(b)}: BPCPDB
- (c) 4-((4-(hexyloxy)phenoxy)carbonyl)phenyl-4-(dimethylamino)benzoate {5(c)}: HPCPDB
- (d) 4-((4-(octyloxy)phenoxy)carbonyl)phenyl-4-(dimethylamino)benzoate {5(d)} : OPCPDB
- (e) 4-((4-(decyloxy)phenoxy)carbonyl)phenyl-4-(dimethylamino)benzoate {5(e)}: DPCPDB
- (f) 4-((4-(dodecyloxy)phenoxy)carbonyl)phenyl-4-(dimethylamino)benzoate {5(f)}:
DdPCPDB
- (g) 4-(dodecyloxy)phenyl-4-(benzoyloxy)benzoate (DdPBB)
- (h) 4-(((4-dodecyloxyphenyl)imino)methyl)phenyl-4-(dimethylamino)benzoate(DdIMPDB)¹⁶
- (i) 4-(((4-(hexyloxy)phenyl)imino)methyl)phenyl-4-(dimethylamino) benzoate (HIMPDB)¹⁶

The experimental protocols and the spectral data of intermediates and the target mesogens are provided in the Electronic Supplementary Information (ESI).

Instrumental details

FT-IR spectra of the compounds were recorded on ABB BOMEM MB3000

spectrometer using KBr pellet. ^1H and ^{13}C solution NMR spectra of the mesogen in CDCl_3 were acquired on a Bruker 400 MHz Avance III HD Nano Bay NMR spectrometer at room temperature using tetramethylsilane (TMS) as an internal standard. The resonance frequencies of ^1H and ^{13}C were 400.23 and 100.64 MHz respectively. Optical polarizing microphotographs were taken using Carl Zeiss Axiocam MRC5 polarizing microscope equipped with a Linkam THMS 600 stage with a TMS 94 temperature programmer. The samples were placed between 12 mm glass cover slips and transferred to heating stage and were heated with a programmed heating rate. The photographs were taken using imager A2M digital camera. Differential scanning calorimetry traces were recorded using a DSC Q200 instrument with a heating rate of $10^\circ\text{C}/\text{min}$ in nitrogen atmosphere. The data obtained from second heating is considered for discussion. UV-visible absorption spectra were measured using Shimadzu UV-1800 spectrophotometer. The steady state fluorescence measurements were carried out by Varian Cary Eclipse fluorescence spectrophotometer.

Computational details

The ground (S_0) geometries of model systems DdPCPDB and DdIMPDB were optimized by density functional theory (DFT) based method with Becke's three-parameter functional and the Lee-Yang-Parr functional (B3LYP)¹⁷⁻¹⁸ with 6-31G* basis set. Based on the gas phase optimized geometry of DdPCPDB, DdIMPDB and DdPBB spectral properties in chloroform were calculated by time dependant density functional theory (TD-DFT) method with Polarizable Continuum Model (PCM) at B3LYP/6-31G* level. All the calculations were carried out using Gaussian 09 program package¹⁹.

Powder X-ray measurements

Powder X-Ray diffraction (XRD) studies of the un-oriented samples (Lindemann capillary, diameter of 1 mm, Hampton Research, Aliso Viejo, CA, USA) were carried out using PANalytical instrument (DY 1042-Empyrean) operating with a line focused Ni-filtered

Cu-K α ($\lambda=1.54 \text{ \AA}$) beam and a linear detector (PIXcel 3D). The sample temperature was controlled with a precision of 0.1 °C using a heater and a temperature controller (Linkam).²⁰

Solid state NMR measurements

The solid-state NMR experiments were carried out on a Bruker Avance III HD 400 WB NMR spectrometer (9.4 T). ^1H and ^{13}C resonance frequencies were 400.07 and 100.61 MHz, respectively. The spectra in the liquid crystalline phases of the sample were recorded using a double resonance 5 mm static probe with a horizontal solenoid coil. For measurement, the sample alignment was achieved by first heating to the isotropic phase and then slowly cooling to the respective mesophases. The proton 90° pulse width was 5 μs . The 1D ^{13}C NMR spectra in SmA_d phase was obtained by cross-polarization (CP) scheme with a 50 kHz radio frequency (RF) field strength on both the ^1H and ^{13}C channels during the contact time of 3 ms, number of scans 128 and a recycle delay of 8 s. High resolution 2D SLF spectra were obtained under static condition using the SAMPI-4 pulse sequence that correlates the ^{13}C chemical shift with the associated ^{13}C - ^1H dipolar coupling. Experimental conditions for SAMPI-4 pulse scheme for liquid crystalline samples were described in our earlier work.²¹ The CP contact time τ was 3 ms, number of t_1 increments was 128 and the signal was acquired with 24 transients for each t_1 increments. The recycle delay of 15 s was used to minimize RF heating effects. The data were zero filled in both the t_2 and t_1 dimensions, yielding a 4096×256 real matrix. A shifted sine bell window function was applied to the time domain data and the spectrum was processed in the phase sensitive mode. SPINAL-64²² heteronuclear decoupling scheme with a 30 kHz RF field strength was used in all the experiments. The sample temperature was regulated by a Bruker BVTB-3500 variable temperature unit and measured from ^{207}Pb NMR chemical shift of $\text{Pb}(\text{NO}_3)_2$.²³ The adamantane methine carbon signal at 29.5 ppm was used as an external reference for ^{13}C chemical shifts calibration.²⁴

3. Results and Discussion

Scheme 1 shows the synthetic route implemented for realising the mesogens. Thus, 4-alkoxy phenols are condensed with 4-dimethylamino benzoyloxy benzoic acid which is prepared from 4-dimethylamino benzoic acid and 4-hydroxy benzaldehyde followed by oxidation. The terminal alkoxy chain is varied from C₂ to C₁₂ with even number carbons only. The structural assignment of all the synthesized mesogens in solution is established by ¹H and ¹³C NMR spectral techniques (Figure S1-S2 of ESI). As stated earlier, the present homologs are structurally similar to recently reported dimethylamino based mesogen series and only differ in the second linking unit¹⁶. The importance of the present work is to explore the photophysical as well as mesophase properties of the current mesogens and compare with those reported recently.¹⁶ Hence, sufficient structural characterization is attempted using the HOPM, DSC, single crystal as well as powder XRD, UV-visible absorption and fluorescence spectroscopy. Further, highest occupied molecular orbital-lowest unoccupied molecular orbital (HOMO-LUMO) by DFT as well as TD-DFT calculations are carried out to get the molecular insight on the photo physical properties. The high resolution solid state ¹³C NMR of representative mesogen (DdPCPDB) is accomplished to get the molecular order.

HOPM, DSC and XRD studies

The synthesised mesogens are investigated using HOPM and DSC to identify and establish the liquid crystalline properties. In HOPM, the samples are taken to isotropic phase and on cooling, the phase formed is identified by noticing the characteristic textures. The existence of nematic phase for all the mesogens is established by seeing the birefringent droplets.²⁵ On further cooling, the droplets coalesced to give threaded texture. For the case of DdPCPDB, the C₁₂ homolog, in addition to nematic phase, SmA_d is also noticed (Figure 1). The sample on cooling the isotropic phase showed threaded nematic texture and at 176.5 °C, the sample changes in to fan texture signifying the phase change.²⁶ The HOPM observations

are supported by DSC studies and accordingly two transitions i.e. crystal-nematic and nematic-isotropic are noted. However, for DdPCPDB, an additional transition at 109.3 °C is observed which is attributed to crystal-SmA_d phase (Figure 2). Table 1 lists the transition temperatures and the enthalpy values of all the synthesized mesogens. The interesting feature of the DSC data is low transition enthalpy for SmA_d to nematic phase indicating pseudo first order nature of the transition. The general trends observed from the HOPM and DSC studies include the progressive decrease in the nematic-isotropic transition temperatures (T_{N-I}) with increase in terminal chain length. Further, the appearance of SmA_d phase only in DdPCPDB is owing to the presence of lengthy dodecyloxy chain which enhances the aspect ratio and favour the segregation of core and terminal chains leading to lamellar order.²⁷ The mesophase range ~70-85 °C for the homologs suggests that the molecular anisotropic polarizability is good. This can be appreciated since the core unit has three phenyl rings that are connected by ester groups which mediate the conjugative interactions. Further, the terminal alkoxy and dimethylamino also enhance the anisotropic interactions in the molecules due to the hetero atoms. A comparison of mesophase transitions of earlier mesogens with the current homologs indicate marginally higher mesophase range for earlier series which could be attributed to the presence of rigid imine link in the core. The SmA_d mesophase range, on the other hand, found to be high for DdPCPDB than DdIMPDB indicating the influence of two ester linking units.

The important and consist feature of the DdIMPDB as well as DdPCPDB is the observation of SmA_d phase for respective C₁₂ homologs. Usually, the interdigitated partial bilayer organization in smectic A phase is noticed for rod-like molecules possessing terminal polar cyano or nitro groups.²⁸ However, the similar organization in dimethylamino based rod-like mesogens is not known in the literature. In order to understand the SmA_d formation in dimethylamino based mesogens, the existing model for the polar mesogens is critically

examined. Due to the presence of nitro or cyano group at one end of the core unit, the terminal dipoles contribute for the overall polarity of the rod-like mesogens. In such mesogens, in order to minimize the dipolar energy, the molecules adopt antiparallel packing leading to smectic A_d formation. Such an arrangement is favored as it provides better way to escape from macroscopic polarity. Similar arguments can be considered for explaining the SmA_d organization in dimethylamino based mesogens. In these molecules owing to the presence of excellent electron donating dimethylamino group, the rest of the core unit acquires negative charge resulting in polarization of the molecules. In order to overcome the dipolar energy, these molecules also adopt antiparallel packing leading to smectic A_d phase. Thus, the main different between the mesogens with polar cyano or nitro versus dimethylamino is the difference in the location of the charge. In other words, in terminal polar mesogens, the negative charge rests on polar group while in mesogens with dimethylamino group, the negative charge locates on the core unit. Hence, the antiparallel packing of neighboring molecules in these mesogens leads to SmA_d organization.

The single crystal structure of BPCPDB is show in Figure 3 and the data is listed in Table 2 (Table S₁-S₇ of ESI). The molecular packing in the crystal leads to triclinic lattice with P1 space group. Interestingly, the HIMPDB, reported recently, also showed triclinic structure. However, the BPCPDB mesogen shows parallel packing with slipped co-facial arrangement whereas HIMPDB exhibited antiparallel packing.¹⁶ Thus subtle alteration in the molecular structure, the spatial arrangement of molecules in crystalline solid state is changed even though the triclinic lattice is common for both the mesogens. Despite the similar crystal lattice, the variation in molecular packing i.e. antiparallel versus parallel packing for HIMPDB and BPCPDB could be argued based on the dipole moment values. The DFT calculations of quantum chemical methods reveal the dipole moments for BPCPDB and HIMPDB as 7.19 D and 4.77 D respectively. Thus the very high dipole moment for BPCPDB

induced by the second ester linking unit could be responsible for slipped co-facial arrangement of the molecules in crystal lattice as against to HIMPDB where anti parallel packing is preferred.

For DdPCPDB which exhibit both nematic and SmA_d phases, the powder X-ray diffraction is carried out in both the phases to further confirm the phase assignment. Figure 4 shows the XRD profile recorded at three different temperatures in SmA_d phase (110-165 °C) while the XRD scan in nematic phase is shown in ESI (Figure S3). In the nematic phase, in the small angle region, no sharp reflection is noticed while a broad hump is clearly observed at wide angle. On the other hand, the XRD profile of SmA_d phase (Figure 4) shows a sharp and intense reflection in small angle region and broad diffuse peak at the wide angle region. The broad hump in the wide angle region indicates the absence of in plane order and liquid like nature of molecules in the layer.²⁹ These features support the layer ordering typical of smectic mesophase.³⁰ The layer spacing (d) determined from small angle reflection at 110 °C, 120°C and 165 °C is found to be 54.46, 53.47 and 51.90 Å respectively. Further, d/L ratios in which L represents the length of the DdPCPDB mesogen (35.48 Å) calculated from energy optimized structure by DFT method of quantum chemical calculations (Figure 5) are in the range of 1.53-1.46 Å. Thus the d/L ratio which is higher than 1.1 and lower than 2 suggest that the phase is partially bilayer smectic A phase (SmA_d).³¹ Further, d-L value for the measurement at 165 °C is found to be 16.42 Å which is equal to the length of dodecyloxy chain. This suggests the antiparallel arrangement of neighboring molecules with overlapping of rigid cores leading to SmA_d organization.

Effect of linking units on twisted intramolecular charge transfer interactions

Intramolecular charge transfer interactions of DdPCPDB and DdIMPDB that originates from N, N-dimethylaminobenzoate moiety and the influence of remotely substituted carboxylate and azomethine groups are studied using computational and experimental meth-

ods. N, N-Dimethylamino benzoate, a well-known molecular probe often discussed for twisted intramolecular charge transfer interactions (TICT) shows characteristic dual emission corresponding to the radiative transition from local excited (LE) state and TICT state.^{32,33} UV-visible absorption spectrum of the compounds DdPCPDB in different solvents with varying polarity (Figure 6). For instance, the measurement in chloroform solvent shows absorption band at 328 nm as depicted in Figure 6. It is clear from the Figure 7 that DdIMPDB exhibit slightly broader absorption band (FWHM=4430 cm^{-1}) as against to DdPCPDB (FWHM=3330 cm^{-1}). The fluorescence spectrum (Figure 8) of DdPCPDB is observed at 366 nm with a shoulder at 433 which is tailing over 500 nm. On the other hand, the fluorescence spectrum of DdIMPDB, is comparatively broad with a maximum at 485 nm. Despite similar chromophoric skeleton, a large red-shift in fluorescence ca. 119 nm for DdIMPDB in contrast to DdPCPDB is really intriguing. This could be due to replacement of carboxylate group of DdPCPDB with azomethine unit in DdIMPDB. The calculated Stokes shifts for DdPCPDB and DdIMPDB respectively are 3540 and 9960 cm^{-1} which suggests that the structural change between the ground and excited state is more predominant for DdIMPDB. Further, the larger Stokes shift for DdIMPDB can also be due to the intramolecular charge transfer interactions between the electron rich N, N-dimethylaminobenzene (donor) and electron deficient ester group (acceptor). Moreover, to understand the intramolecular charge transfer interactions, solvent polarity dependent fluorescence spectral studies are carried out. In our recent report, it is observed that DdIMPDB with N, N-dimethylaminobenzoate moiety does not show any dual emission, a characteristic feature of TICT interactions.¹⁶ Indeed DdIMPDB exhibit negative solvatochromism in fluorescence, a rare phenomenon, suggesting a large dipole moment in the ground state than in the excited state. On the other hand, DdPCPDB shows progressive red-shift in fluorescence while going from nonpolar toluene to polar acetonitrile solvent. Interestingly, only one emission peak is observed in hexane, toluene and methanol respectively

at 344, 358 and 367 nm, while in ethyl acetate, dichloromethane, chloroform, tetrahydrofuran, acetonitrile and dimethyl sulfoxide, two peaks are found characteristic to the nature of the solvent. The higher energy emission originates from the local excited (LE) state or Franck Condon state and the anomalous, second emission peak observed at longer wavelength region would have been originated from the TICT state. The ratio of the relative intensity between the TICT and LE state is also found to depend upon the solvent. Particularly, in ethyl acetate, dichloromethane, chloroform, tetrahydrofuran, acetonitrile and dimethylsulfoxide higher ratio is noticed in contrast to other non-polar solvents. The subtle structural differences between DdPCPDB and DdIMPDB, though not directly linked to the N, N-dimethylamino benzoate has drastic changes in the intramolecular charge transfer interactions. To get more insight in to the experimental findings, DFT and TD-DFT calculations are conducted with the Gaussian 09 program using the B3LYP method and 6-31G* basis set. Figure 9 displays the optimized molecular structures wherein, the phenyl rings are designated as A, B, and C for clarity. As can be seen from the dihedral angles summarized in Table 3, almost similar value is observed between the ring A and B. This suggests that neither ester nor azomethine between B and C exerts geometrical impact on dimethylamino benzoate group. However, the dihedral angle between rings B and C ($C_9-O_{10}-C_{11}-C_{12}$) is found to vary significantly from 150° to 132° . It is clear that, ester substituted mesogens (DdPCPDB and DdPBB) loses co-planarity at ring B which in turn reduces the extended π -conjugation in contrast to imine based mesogen (DdIMPDB). As a result of loss of co-planarity in DdPCPDB, the ring B and C with delocalized π -conjugation acts as a chromophoric unit, whereas for DdPCPDB and DdPBB, the ring A and B are responsible for electronic properties. These findings are akin with frontier orbital contour plots as shown in Figure 10. For mesogens DdPCPDB, the HOMO is localized on N, N-dimethylaminobenzene moiety, and LUMO is predominantly concentrated on the phenyl benzoate unit. In the case of DdIMPDB and DdPBB, the HOMO is concentrated on the ben-

zylidene-phenyl unit, whereas LUMO is delocalized on the phenyl benzoate moiety. For all the cases, the HOMO→LUMO transition induces significant redistribution of electron density due to intramolecular charge transfer interactions with characteristic to the nature of the substituent.

TD-DFT calculations are also performed to find out the orbitals involved in the dominant excited state electronic transitions and their corresponding energies and oscillator strength and the results are listed in Table 4. A close analysis of these values shows that the calculated spectral properties of both the model systems are in close agreement with experimental values. In all the systems (DdPCPDB, DdIMPDB and DdPBB), the charge transfer peak is observed at 340.3, 320.5 and 320.2 nm respectively, which constitutes the HOMO→LUMO transition (Table 5).

High Resolution Solid State ^{13}C NMR Spectroscopy

The solution proton decoupled ^{13}C NMR spectrum of DdPCPDB (CDCl_3) is shown in Figure 11(a) where well resolved lines are seen from 14-165 ppm. In the range 110-165 ppm, 14 lines with varying intensities arising from the core unit carbons are observed. Among them, six lines with comparable intensity are assigned to three phenyl ring CH carbons. The remaining low intense lines are due to quaternary carbons of phenyl ring as well as ester carbonyl carbons. The individual assignment of all the carbons are carried out by making use of ^{13}C chemical shifts computed from DFT calculations. Table 6 list the experimental ^{13}C chemical shifts as well as those calculated from DFT method of core unit carbons. For the terminal units i.e. dodecyloxy chain and dimethylamino carbons, the lines have appeared in the range 14-69 ppm. Of them, the OCH_2 carbon of dodecyloxy chain is easily identified at 68.4 ppm whereas the methyl carbons of dimethylamino unit are seen at 40.0 ppm. The terminal methyl carbon of the dodecyloxy chain is noted at 14.1 ppm and rest of the methylene carbons are noticed in the range 22-32 ppm.

The static ^{13}C NMR spectra of DdPCPDB recorded in SmA_d phase at 115°C and 155°C are shown in Figure 11 (b) & (c). As the mesogen exhibits narrow nematic mesophase range ($\sim 8^\circ\text{C}$) than SmA_d phase ($\sim 67^\circ\text{C}$), the ^{13}C NMR experiments are performed only in SmA_d phase. The spectrum shows 9 peaks in the range 132-234 ppm contributed by core unit carbons arising from phenyl rings as well as ester linking units. The peaks appeared in the range 132-165 ppm are relatively more intense than the remaining (173-234 ppm) peaks. These high intense signals are assigned to phenyl ring methine carbons of core units. In solution ^{13}C NMR spectrum, six lines are clearly observed for the methine carbons of three phenyl rings of the core unit. The less number of peaks observed in the static spectrum indicates that some of the carbons are overlapping due to the similar chemical environment. The complete assignment of the spectrum is carried out by making use of ^{13}C NMR data of recently published mesogen as well as with the use of 2D SLF spectrum.¹⁶ For the terminal chain carbons, the peaks are observed in the range 11-63 ppm. Among them, the distinguishable peaks are from OCH_2 carbon (62.2 ppm), methyl carbons of dimethyl group (40.5 ppm) and terminal methyl carbon (11.5 ppm). The methylene carbons of dodecyloxy chain, on the other hand, are noticed in the range 20-28 ppm. It is clear from the comparison of chemical shift values of solution and static ^{13}C NMR spectrum that in SmA_d phase, the molecules are aligned in the magnetic field. Further, increase in the chemical shifts of core unit carbons and a marginal decrease for the terminal chain carbons indicate that the alignment of the long axis is parallel to the magnetic field.³⁴ Similar trends are noticed for the static spectrum measured at 155°C in SmA_d and the corresponding chemical shift values are listed in the Table 6.

The 2D solid state ^{13}C NMR of DdPCPDB is carried out in SmA_d phase with a view to find the molecular order using the ^{13}C - ^1H dipolar couplings. Typically the 2D spectrum provides the information about the carbon chemical shift and ^{13}C - ^1H dipolar couplings which can be utilized to find the order parameter of phenyl rings of the core unit. The 2D spectra

measured at 115 °C and 155 °C in SmA_d phase are shown in Figure 12 (a) & (b). Similar to the 1D static spectrum, the 2D also shows 9 contours in the range 132-234 ppm which are mainly arising from core unit carbons. The important features of the 2D spectra is observation of four contours for phenyl ring methine carbons in the range 132-165 ppm among which the contours appeared at 164.3 and 152.6 ppm are more intense and is due to the overlapping of C₃ and C₈ as well as C₇ and C₁₂ carbons respectively. A close examination of 2D spectrum in the range 204-210 ppm, however, shows low intense contours from ester linking units. The chemical shift assignment of ring I carbons is carried out using the ¹³C NMR data of recently reported mesogen which also shows SmA_d phase and has structurally similar ring I.¹⁶ For ring III also ¹³C NMR data in liquid crystalline phase is available from the literature.³⁵ Table 6 lists the ¹³C-¹H dipolar couplings of core unit carbons measured in SmA_d phase at two different temperatures.

By making use of ¹³C-¹H dipolar couplings and employing the equation 1 mentioned below, the order parameter of the phenyl rings of the core unit is determined. The method adopted for extracting the dipolar couplings from experimentally determined dipolar oscillation frequency and their use for determining the order parameter is briefly mentioned. The dipolar oscillation frequency corresponds directly to the dipolar coupling only for an isolated C-H pair whereas for a carbon coupled to more than one proton, the dipolar couplings have to be extracted from the oscillation frequency. For instance, in the case of phenyl ring methine carbons, the experimental dipolar frequency has two contributions namely, a coupling to the attached proton D_{C-Hi} and also a coupling to the remote proton at the ortho position D_{C-Ho}. Then the measured frequency is given by $[(D_{C-Hi})^2 + (D_{C-Ho})^2]^{1/2}$.³⁶ For the case of quaternary carbons, couplings to two equivalent protons at the ortho positions are possible and hence the dipolar frequency will be $\sqrt{2} * (D_{C-Ho})$. Further, these dipolar couplings are related to the local order parameters, namely, S_{zz} and (S_{xx}-S_{yy}) by the following

equation,³⁷

$$D_{CH}=K [1/2 (3 \cos^2\theta_z-1) S_{zz}+ 1/2 (\cos^2\theta_x - \cos^2\theta_y) (S_{xx} - S_{yy})] \quad (1)$$

where $K=-h\gamma_H\gamma_C/4\pi^2r_{CH}^3$, with γ_H and γ_C are the gyromagnetic ratios of 1H and ^{13}C nuclei respectively, r_{CH} is the inter-nuclear vector, θ_x , θ_y and θ_z are angles between r_{CH} and the corresponding molecular axes. For the phenyl rings, the molecular frame is defined by taking para-axis (C_2 axis) as the z-axis, the x-axis is in the plane of the ring while the y-axis is perpendicular to the plane. Further, the standard bond distances of $r_{CH} = 1.1 \text{ \AA}$ for the C–H bond and $r_{CC} = 1.4 \text{ \AA}$ for the C–C bond are considered. In order to arrive at the best fit, the two C–C–H bond angles are also varied slightly $\sim 120^\circ$. By employing the equation 1, the local order parameters S_{zz} and $(S_{xx}-S_{yy})$ are calculated from the experimentally determined dipolar frequencies for each of the phenyl rings at different temperatures in SmA_d phase and are listed in Table 7. It is clear from the Table 7 that the ring II order parameter is slightly higher than ring I as well as ring III, a trend normally encountered in three ring mesogens.^{38, 39} The S_{zz} values are in consistent with the literature data of those rod-like mesogens that exhibit SmA_d phase.^{5, 39}

Since the 1D static ^{13}C experiments are carried out at different temperatures covering SmA_d phase for DdPCPDB, AIS vs Temperature data is plotted as shown in Figure 13. It is clear from the plot that with increase in temperature a decrease in AIS values is noticed. The trend observed in the plot is in consistent with the order parameters calculated from ^{13}C - 1H dipolar couplings. It is pertinent to mention that in a recent work, Domenici et al have investigated the ^{13}C NMR of three ring mesogens which shows smectic Devries phase. The study revealed that at the phase transition temperature, conformational change of the molecules is clearly noticed. However, in the present work such conformation change is not observed with in the SmA_d phase for which the chemical shift data is available.

4. Conclusion

Thermotropic mesogens with dimethylamino connected to three phenyl ring core with terminal alkoxy chain were synthesised from 4-dimethylamino benzoic acid. The mesophase investigations revealed enantiotropic nematic phase for all the homologs and additional SmA_d phase for C₁₂ homolog. The powder X-ray diffraction studies unequivocally support the interdigitated bilayer organization in smectic A phase. In these molecules owing to the presence of excellent electron donating dimethylamino group, the rest of the core unit acquires negative charge resulting in polarization of the molecules. In order to overcome the dipolar energy, these molecules adopt antiparallel packing leading to the formation partial bilayer smectic A organization. Further, the slipped co-facial arrangement of molecules in crystal lattice for BPCPDB is attributed to high dipole moment (7.19 D) in contrast to C6 mesogen of earlier series. Interestingly, UV-visible and fluorescence spectroscopy accompanied by computational methods disclose the existence of twisted intramolecular charge transfer state. Further the computational methods provided the information about the dihedral angles between the rings which were correlated to the delocalized π -conjugation of chromophoric unit. The TD-DFT calculations disclosed the orbitals involved in the dominant excited state electronic transitions and their corresponding energies together with oscillator strength. A close scrutiny of these values shows that the calculated spectral properties of both the systems were found to be in close agreement with experimental values. Thus the charge transfer peak observed at 340.3, 320.5 and 320.2 nm respectively were originated from HOMO→LUMO. The orientational order parameters of the core unit in SmA_d phase determined from the high resolution solid state ¹³C NMR are found to be 0.71 and 0.64 at 115°C and 155°C.

Electronic supplementary information (ESI)

It contains the synthetic details, experimental details, single crystal data and check file

for BPCPDB, ^1H , ^{13}C NMR spectra of synthesized mesogens and powder X-ray diffraction profile for DdPCPDB in nematic phase at 180 °C.

Acknowledgments

The authors thank Dr. A. B. Mandal, Outstanding Scientist, CLRI and Prof. K. V. Ramanathan, NMR Research Centre, Indian Institute of Science, Bangalore, India for their support and keen interest in this work. The authors are thankful to Dr. V. Subramanian, CLRI, for his help and support. We are also indebted to Prof. V. A. Raghunathan and Ms. K. N. Vasudha, Raman Research Institute, Bangalore, India for the powder X-ray measurements. The partial financial support from NWP-55 is duly acknowledged. MGR thanks Council of Scientific and Industrial Research (CSIR), New Delhi for Senior Research Fellowship.

Notes and References

- 1 C. Tschierske, *Liquid Crystals: Materials Design and Self-assembly*, Springer-Verlag, Berlin Heidelberg, 2012.
- 2 (a) C. Tschierske, *Angew. Chem. Int. Ed.*, 2013, **52**, 8828-8878; (b) T. Kato, N. Mizoshita and K. Kishimoto, *Angew. Chem. Int. Ed.*, 2006, **45**, 38-68.
- 3 (a) M. Lehmann, *Top. Curr. Chem.*, 2012, **318**, 193-223; (b) R. Amaranatha Reddy and C. Tschierske, *J. Mater. Chem.*, 2006, **16**, 907-961.
- 4 (a) M. Funahashi and T. Kato, *Liq. Cryst.*, 2015, **42**, 909-917; (b) J. W. Goodby, R. J. Mandle, E. J. Davis, T. Zhong and S. J. Cowling, *Liq. Cryst.*, 2015, **42**, 593-622.
- 5 (a) M. Kesava Reddy, K. Subramanyam Reddy, K. Yoga, M. Prakash, T. Narasimhaswamy, A. B. Mandal, N. P. Lobo, K. V. Ramanathan, D. S. Shankar Rao and S. Krishna Prasad, *J. Phys. Chem. B*, 2013, **117**, 5718-5729; (b) N. P. Lobo, B. B. Das, T. Narasimhaswamy and K. V. Ramanathan, *RSC Adv.*, 2014, **4**, 33383-33390.
- 6 (a) G. R. Luckhurst and G. W. Gray, *The Molecular Physics of Liquid Crystals*; Academic Press: New York, 1979; (b) P. J. Collings and M. Hird, *Introduction to Liquid Crystals Chemistry and Physics*; Taylor and Francis: London, 1997.
- 7 (a) F. Hardouin and A. M. Levelut, *J. Physique*, 1980, **41**, 41-46 ; (b) A. J. Lead better, J. C. Frost, J. P. Gaughan, G. W. Gray and A. Mosley, *J. Physique*, 1979, **40**, 375-380; (c) F. Hardouin, A. M. Levelut and G. Sigaud, *J. Physique*, 1981, **42**, 71-77.
- 8 (a) N. H. Tinh, F. Hardouin, C. Destrade and A.M. Levelut, *J. Physique Lett.*, 1982, **43**, 33-37; (b) F. Hardouin, G. Sigaud, N. H. Tinh and M.F. Achard, *J. Physique Lett.*, 1981, **42**, 63-66.
- 9 C. T. L. Chan, C. C. W. Cheng, K. Y. Fung Ho and W. M. Kwok, *Phys. Chem. Chem. Phys.*, 2011, **13**, 16306-16313.
- 10 A. Ito, S. Ishizaka and N. Kitamura, *Phys. Chem. Chem. Phys.*, 2010, **12**, 6641-6649.

- 11 W. Rettig, *Angew. Chem. Int. Ed.*, 1986, **25**, 971-988.
- 12 C. Zhong, *Phys. Chem. Chem. Phys.*, 2015, **17**, 9248-9257.
- 13 (a) K. Praefcke and D. Singer, *Charge Transfer Systems*. In *Hand Book of Liquid Crystals*; D. Demus, J. W. Goodby, G. W. Gray, H. W. Spiess and V. Vill, Eds.; (Weinheim, Wiley-VCH) Germany, 1998; Vol. 2B, pp 945-967; (b) T. Narasimhaswamy and K. S. V. Srinivasan, *Liq. Cryst.*, 2004, **31**, 1457-1462; (c) T. Narasimhaswamy, M. Monette, D. K. Lee and A. Ramamoorthy, *J. Phys. Chem. B*, 2005, **109**, 19696-19703.
- 14 (a) M. Liang and J. Chen, *Chem. Soc. Rev.*, 2013, **42**, 3453-3488; (b) B. Carloti, E. Benassi, A. Cesaretti, C.G. Fortuna, A. Spalletti, V. Barone and F. Elisei, *Phys. Chem. Chem. Phys.*, 2015, **17**, 20981-20989.
- 15 (a) H. Xiao, J. Miao, J. Cao, W. Yang, H. Wu and Y. Cao, *Org. Electron.*, 2014, **15**, 758-774; (b) Z. Jiang, Z. Zhong, S. Xue, Y. Zhou, Y. Meng, Z. Hu, Na Ai, J. Wang, L. Wang, J. Peng, Y. Ma, J. Pei, J. Wang and Y. Cao, *ACS Appl. Mater. Interfaces*, 2014, **6**, 8345-8352; (c) A. Das and S. Ghosh, *Angew. Chem. Int. Ed.*, 2014, **53**, 2038-2054.
- 16 M. Guruprasad Reddy, E. Varathan, N. P. Lobo, S. Easwaramoorthi, T. Narasimhaswamy and A. B. Mandal, *J. Phys. Chem. C*, 2015, **119**, 9477-9487.
- 17 A. D. Becke, *J. Chem. Phys.*, 1993, **98**, 5648-5652.
- 18 B. Lee, W. Yang and R. G. Parr, *Phys. Rev. B*, 1988, **37**, 785-789.
- 19 M. J. Frisch, G. W. Trucks, H. B. Schlegel, G. E. Scuseria, M. A. Robb, J. R. Cheeseman, G. Scalmani, V. Barone, B. Mennucci, G. A. Petersson, et al. GAUSSIAN 09, Revision A.02; Gaussian, Inc. Wallingford, CT, 2009.
- 20 (a) S. K. Gupta, S. Setia, S. Sidiq, M. Gupta, S. Kumar and S. K. Pal, *RSC Adv.*, 2013, **3**, 12060-12065; (b) S. Radhika, M. Monika, B. K. Sadasiva and A. Roy, *Liq. Cryst.*, 2013, **40**, 1282-1295.

- 21 (a) N. P. Lobo, M. Prakash, T. Narasimhaswamy and K. V. Ramanathan, *J. Phys. Chem. A*, 2012, **116**, 7508-7515; (b) M. Kesava Reddy, E. Varathan, N. P. Lobo, B. B. Das, T. Narasimhaswamy and K. V. Ramanathan, *J. Phys. Chem. C*, 2014, **118**, 15044-15053; (c) B. B. Das, T. G. Ajitkumar and K. V. Ramanathan, *Solid State Nucl. Magn. Reson.*, 2008, **33**, 57-63.
- 22 B. M. Fung, A. K. Khitrin and K. Ermolaev, *J. Magn. Reson.*, 2000, **142**, 97-101.
- 23 P. A. Beckmann and C. Dybowski, *J. Magn. Reson.* 2000, **146**, 379-380.
- 24 A. McDermott and Z. Gu, *Carbon & Nitrogen Chemical Shifts of Solid State Enzymes* in *Encyclopedia of Nuclear Magnetic Resonance*, Advances in NMR, Eds. D. M. Grant and R. K. Harris, Columbia University, New York, USA, Volume 9.
- 25 I. Dierking, *Textures of Liquid Crystals*, Wiley-VCH Verlag GmbH, Weinheim, Germany, 2003.
- 26 G. W. Gray and J. W. Goodby, *Smectic Liquid Crystals: Textures and Structures*; Leonard Hill: London, 1984.
- 27 D. Guillon, G. Poeti, A. Skoulios and E. Fanelli, *J. Physique Lett.*, 1983, **44** 491-494.
- 28 (a) D. Guillon and A. Skoulios, *Mol. Cryst. Liq. Cryst.*, 1983, **91**, 341-352; (b) A. J. Leadbetter, J. C. Frost, J. P. Gaughan, G. W. Gary and A. Mosley, *J. Phys.*, 1979, **40**, 375-380.
- 29 J. M. Seddon, *Structural Studies of Liquid Crystals by X-Ray Diffraction*. In *Hand Book of Liquid Crystals*; Eds. D. Demus, J. W. Goodby and G. W. Gray, H. W. Spiess and V. Vill, Wiley-VCH: Weinheim, Germany, 1998; Vol. 1, pp 635-679.
- 30 A. De Vries, *Mol. Cryst. Liq. Cryst.*, 1985, **131**, 125-145.
- 31 (a) F. Hardouin, *Phys. A (Amsterdam, Neth.)*, 1986, **140**, 359-367; (b) R. Dąbrowski, *Liq. Cryst.*, 2015, **42**, 783-818.

- 32 W. Huang, X. Zhang, L. H. Ma, C. J. Wang and Y. B. Jiang, *Chem. Phys. Lett.*, 2002, **352**, 401-407.
- 33 Z. R. Grabowski and K. Rotkiewicz, *Chem. Rev.*, 2003, **103**, 3899-4032.
- 34 (a) R. Y. Dong, *Nuclear Magnetic Resonance Spectroscopy of Liquid Crystals*; World Scientific: Singapore, 2010; (b) *Thermotropic Liquid Crystals: Recent Advances*, ed. A. Ramamoorthy, Springer, Dordrecht, Netherlands, 2007, p. 38; (c) V. Domenici, M. Geppi and C. A. Veracini, *Prog. Nucl. Magn. Reson. Spectrosc.*, 2007, **50**, 1-50.
- 35 B. Veeraprakash, N. P. Lobo, T. Narasimhaswamy and A. B. Mandal, *Phys. Chem. Chem. Phys.*, 2015, **17**, 19936-19947.
- 36 M. Kesava Reddy, K. Subramanyam Reddy, T. Narasimhaswamy, B. B. Das, N. P. Lobo and K. V. Ramanathan, *New J. Chem.*, 2013, **37**, 3195-3206.
- 37 (a) J. Xu, K. F. Csorba and R. Y. Dong, *J. Phys. Chem. A*, 2005, **109**, 1998-2005; (b) B. M. Fung, *Prog. Nucl. Magn. Reson. Spectrosc.*, 2002, **41**, 171-186; (c) B. M. Fung, *En-cycl. Nucl. Magn. Reson.*, 1996, **4**, 2744-2751.
- 38 S. Kalaivani, T. Narasimhaswamy, B. B. Das, N. P. Lobo and K. V. Ramanathan, *J. Phys. Chem. B*, 2011, **115**, 11554-11565.
- 39 (a) M. Cifelli, V. Domenici and C. A. Veracini, *Curr. Opin. Colloid & Interface Sci.*, 2013, **18**, 190-200; (b) A. Marchetti, V. Domenici, V. Novotna, M. Lelli, M. Cifelli, A. Lesage, and C. A. Veracini, *Chem. Phys. Chem.*, 2010, **11**, 1641-1645; (c) V. Domenici, M. Lelli, M. Cifelli, V. Hamplova, A. Marchetti, and C. A. Veracini, *Chem. Phys. Chem.*, 2014, **15**, 1485-1495; (d) R. Y. Dong, J. Xu, J. Zhang and C. A. Veracini, *Phys. Rev. E: Stat., Nonlinear, Soft Matter Phys.*, 2005, **72**, 061701(1-8); (e) R. Y. Dong, *Annu. Rep. NMR Spectrosc.*, 2015, DOI:10.1016/bs.arnmr.2015.05.001.

Table 1: Transition temperatures and enthalpy values of synthesized mesogens 5(a-f)^a.

Code	T _{C-N/C-SmAd} (°C)	ΔH (k.cal/mol)	T _{SmAd-N} (°C)	ΔH (k.cal/mol)	ΔT T _{SmAd-N}	T _{N-I} (°C)	ΔH (k.cal/mol)	ΔT T _{N-I}
EPCPDB	192.2	8.76	-	-	-	262.4	0.41	70.2
BPCPDB	161.7	6.80	-	-	-	233.7	0.33	72.0
HPCPDB	121.2	4.04	-	-	-	205.8	0.31	84.6
OPCPDB	114.7	9.22	-	-	-	194.1	0.28	79.4
DPCPDB	112.8	8.55	-	-	-	186.4	0.26	73.6
DdPCPDB	109.3	6.47	176.5	0.0196	67.2	185.2	0.24	8.7

^aC-Crystal; SmA_d Interdigitated bilayer smectic A; N-Nematic; I-Isotropic.

Table 2: Single crystal data for BPCPDB

Identification code	BPCPDB
Empirical formula	C ₂₆ H ₂₇ NO ₅
Formula weight	433.49
Temperature	293(2) K
Wavelength	0.71073 Å
Crystal system, space group	Triclinic, P-1
Unit cell dimensions	a = 9.8058(2) Å alpha = 64.9330(10) deg. b = 15.4400(3) Å beta = 83.4090(10) deg. c = 16.9339(3) Å gamma = 88.3180(10) deg.
Volume	2306.46(8) Å ³
Z, Calculated density	4, 1.248 Mg/m ³
Absorption coefficient	0.086 mm ⁻¹
F(000)	920
Crystal size	0.20 x 0.15 x 0.10 mm
Theta range for data collection	1.34 to 26.45 deg.
Limiting indices	-12 ≤ h ≤ 12, -18 ≤ k ≤ 19, -21 ≤ l ≤ 21
Reflections collected / unique	35532 / 9485 [R(int) = 0.0644]
Completeness to theta = 26.45	99.6 %
Absorption correction	Semi-empirical from equivalents
Max. and min. transmission	0.9914 and 0.9829
Refinement method	Full-matrix least-squares on F ²
Data / restraints / parameters	9485 / 0 / 583
Goodness-of-fit on F ²	0.927
Final R indices [I > 2σ(I)]	R1 = 0.0510, wR2 = 0.1038
R indices (all data)	R1 = 0.1539, wR2 = 0.1445
Largest diff. peak and hole	0.206 and -0.174 e.Å ⁻³
CCDC No.:	1415623

Table 3: Calculated Dihedral Angles using B3LYP/6-31G* optimized geometries.

Compounds	Dihedral Angle			
	C ₁ -C ₂ -C ₃ -O ₄	C ₃ -O ₄ -C ₅ -C ₆	C ₇ -C ₈ -C ₉ -O ₁₀	C ₉ -O ₁₀ -C ₁₁ -C ₁₂
DdPCPDB	179	141	179	132
DdIMPDB	179	142	178	150
DdPBB	178	140	179	132

Table 4: Summary of the excited state electronic transitions obtained from the TD-DFT calculations at B3LYP/6-31G* level.

Compounds	Solvent	States	Absorption (nm)	Energy (eV)	Oscillator strength (f)	Dominant contribution (%) ^a	Exp. (nm)
DdPCPDB	CHCl ₃	S ₁	340.3	3.64	0.4324	H→L (98%)	328
		S ₂	390.4	3.88	0.1255	H-1→L (94%)	
		S ₃	291.9	4.25	0.6476	H→L+1(94%)	
DdIMPDB	CHCl ₃	S ₁	320.5	3.87	0.9480	H→L (67%), H→L+1(18%)	328
		S ₂	266.3	4.66	0.6233	H-1→L (38%), H-6→L (28%)	
DdPBB	CHCl ₃	S ₁	330.2	3.75	0.1335	H→L (90%)	338
		S ₂	270.0	4.59	0.5681	H→L (94%)	
		S ₃	241.3	5.14	0.2942	H-5→L (55%), H-1→L+1(34%)	

^a H denotes HOMO and L denotes LUMO.

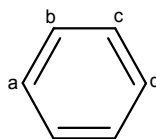
Table 5: Calculated HOMO, LUMO and HOMO-LUMO gap ($\Delta_{\text{H-L}}$) at B3LYP/6-31G* level

Compounds	HOMO	LUMO	$\Delta_{\text{H-L}}$
DdPCPDB	-5.55	-1.26	4.28
DdIMPDB	-5.22	-1.34	3.89
DdPBB	-5.75	-1.65	4.09

Table 6: ^{13}C NMR data of DdPCPDB in solution and liquid crystalline state^a

C. No	Solution (ppm)	DFT (ppm)	115°C			155°C		
			SmA _d phase (ppm)	AIS (ppm)	^{13}C - ^1H Dipolar Oscillation Frequencies (kHz)	SmA _d phase (ppm)	AIS (ppm)	^{13}C - ^1H Dipolar Oscillation Frequencies (kHz)
1	153.9	150.4	219.1	65.2	1.64	211.1	57.2	1.49
2	110.8	108.3	132.4	21.6	3.19	130.2	19.4	2.81
3	132.2	132.6	164.3	32.1	2.71	159.8	27.6	2.44
4	115.3	116.5	178.1	62.8	1.59	170.9	55.6	1.44
5	164.9	161.6	209.0	44.1	0.60	203.0	38.1	0.64
6	155.7	156.3	214.7	59.0	1.63	205.9	50.2	1.47
7	122.4	121.1	152.6	30.2	2.58	148.0	25.6	2.36
8	131.7	132.0	163.9	32.2	2.71	159.8	28.1	2.44
9	126.7	125.3	198.0	71.3	1.65	188.7	62.0	1.52
10	165.0	162.6	204.6	39.6	0.56	200.2	35.2	0.99
11	144.2	144.7	214.7	70.5	1.63	205.9	61.7	1.47
12	122.2	123.9	152.3	30.1	2.58	148.0	25.8	2.36
13	115.1	116.1	142.5	27.4	2.80	139.0	23.9	2.50
14	156.9	156.1	233.4	76.5	1.64	223.9	67.0	1.48

^a DFT-Density functional theory; CS-Chemical shifts; AIS; Aligned induced chemical shifts.

Table 7: Orientational order parameter values of DdPCPDB

T (°C)	Ring	Angles		S_{zz}	$(S_{xx} - S_{yy})$	Calculated Dipolar Oscillation Frequencies (kHz)				RMSD (kHz)
		θ_b	θ_c			b	c	a	d	
115	I	119.3	120.7	0.70	0.068	3.18	2.74	1.59	1.63	0.03
	II	121.2	120.8	0.71	0.066	2.59	2.72	1.66	1.65	0.02
	III	121.2	120.5	0.70	0.070	2.59	2.81	1.65	1.63	0.01
155	I	119.5	120.8	0.63	0.062	2.81	2.44	1.44	1.47	0.03
	II	121.1	120.9	0.64	0.058	2.36	2.41	1.49	1.49	0.03
	III	121.0	120.5	0.63	0.060	2.37	2.51	1.47	1.46	0.01

Figure Captions:

Scheme 1 Synthetic route adopted for realizing mesogens

Figure 1: HOPM photographs of DdPCPDB on cooling the isotropic phase (a) Birefringence nematic droplets at 185.1 °C, (b) Nematic threads at 178.0 °C (c) Nematic to SmA_d Phase transition at 176.0 °C and (d) Fan texture of SmA_d at 138.3 °C

Figure 2: DSC second heating and cooling scans of DdPCPDB

Figure 3: ORTEP diagram of BPCPDB

Figure 4: Powder X-ray diffraction profile for DdPCPDB SmA_d phase(a) at 110 °C, (b) at 120 °C, and (c) at 165 °C

Figure 5: (a) Molecular structure and (b) Energy optimized space filled model, magnitude and direction of dipole moment of DdPCPDB

Figure 6: Solution absorption spectra of DdPCPDB in different solvents with varying polarity

Figure 7: UV-visible absorption (solid line) and fluorescence (dashed line) spectra of compounds DdPCPDB and DdIMPDB in chloroform. The fluorescence spectra recorded by exciting the samples at their respective absorption maximum wavelength

Figure 8: Solution fluorescence spectra of DdPCPDB in different polarity solvents

Figure 9: Optimized geometries of DdPCPDB, DdIMPDB and DdPBB at B3LYP/6-31G8 level of theory

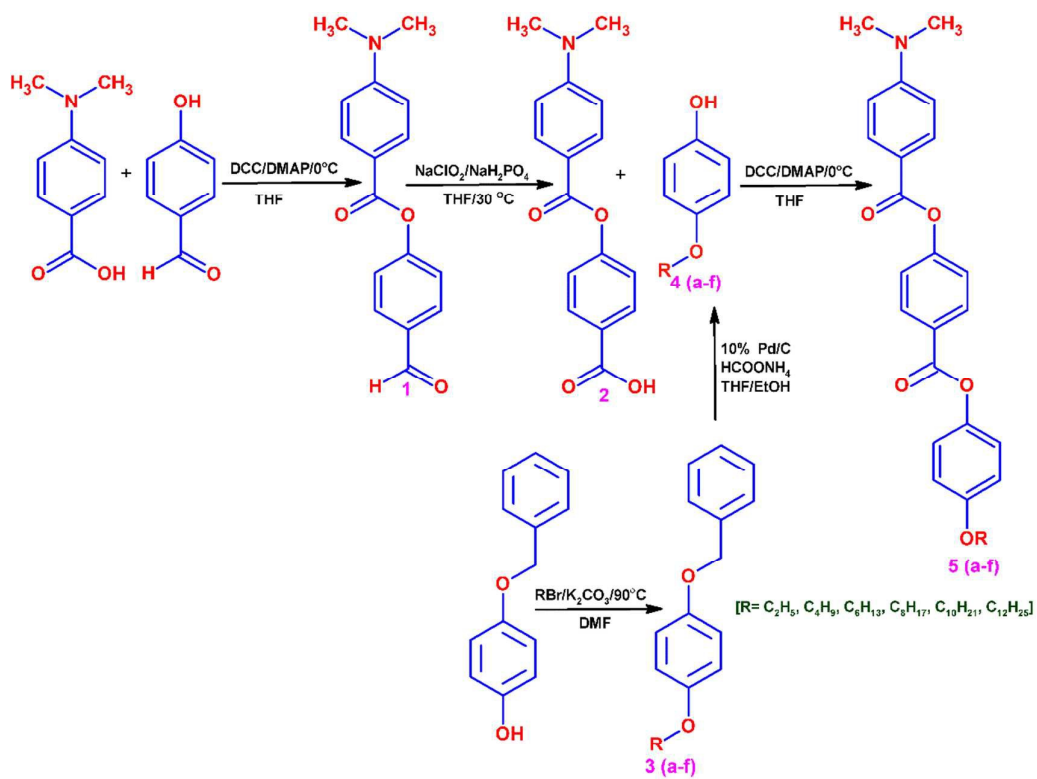
Figure 10: FMO distribution of DdPCPDB and DdIMPDB (isosurface value = 0.03 au) at B3LYP/6-31G* level of theory

Figure 11: ¹³C NMR spectra of DdPCPDB in (a) solution, (b) SmA_d phase at 115 °C and (c) at 155 °C

Figure 12: 2D SAMPI-4 spectra of DdPCPDB in SmA_d phase (a) at 115 °C and (b) at 155 °C

Figure 13: Plot of temperature versus alignment induced chemical shifts (AIS) in SmA_d of DdPCPDB

Scheme 1



Scheme 1

Figure 1

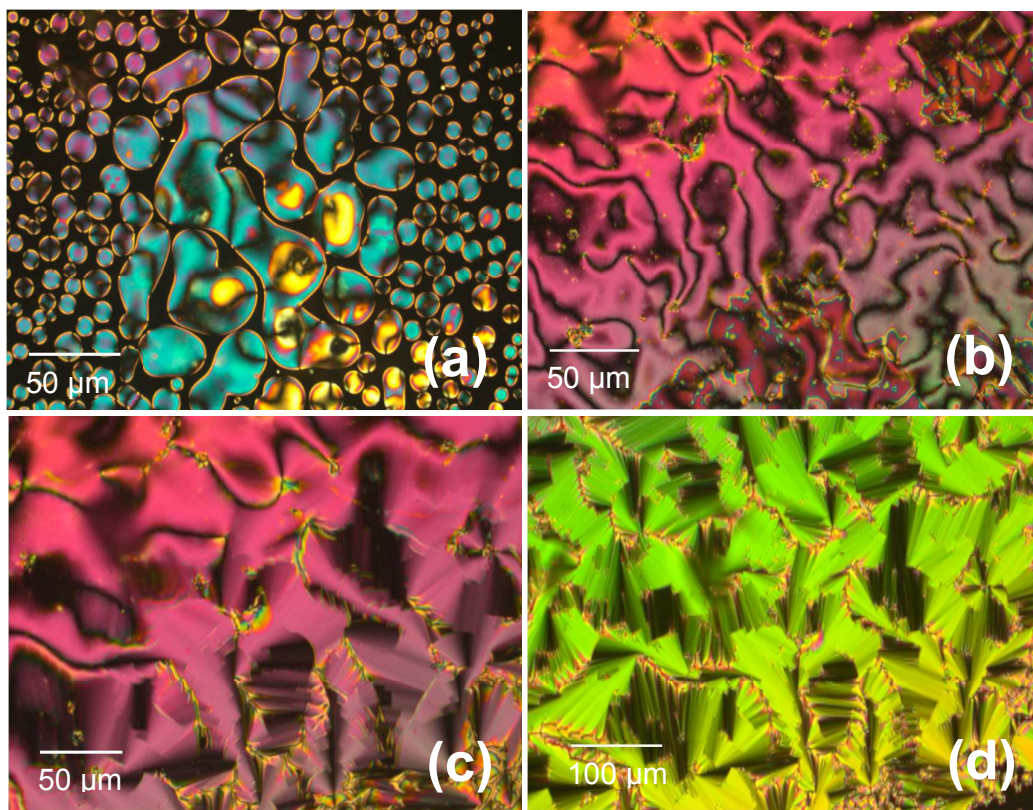


Figure 2

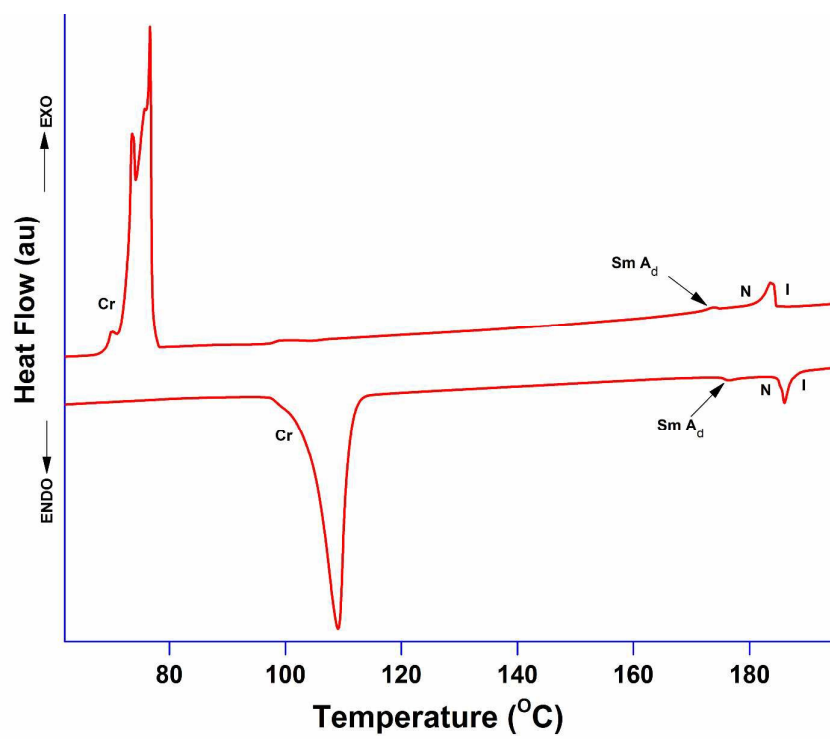


Figure 3

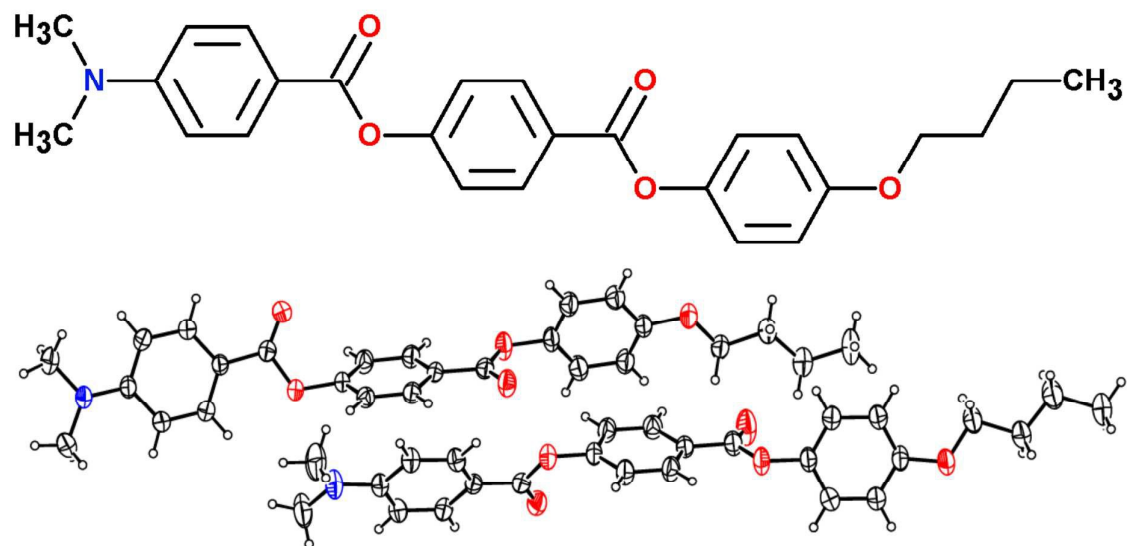


Figure 4

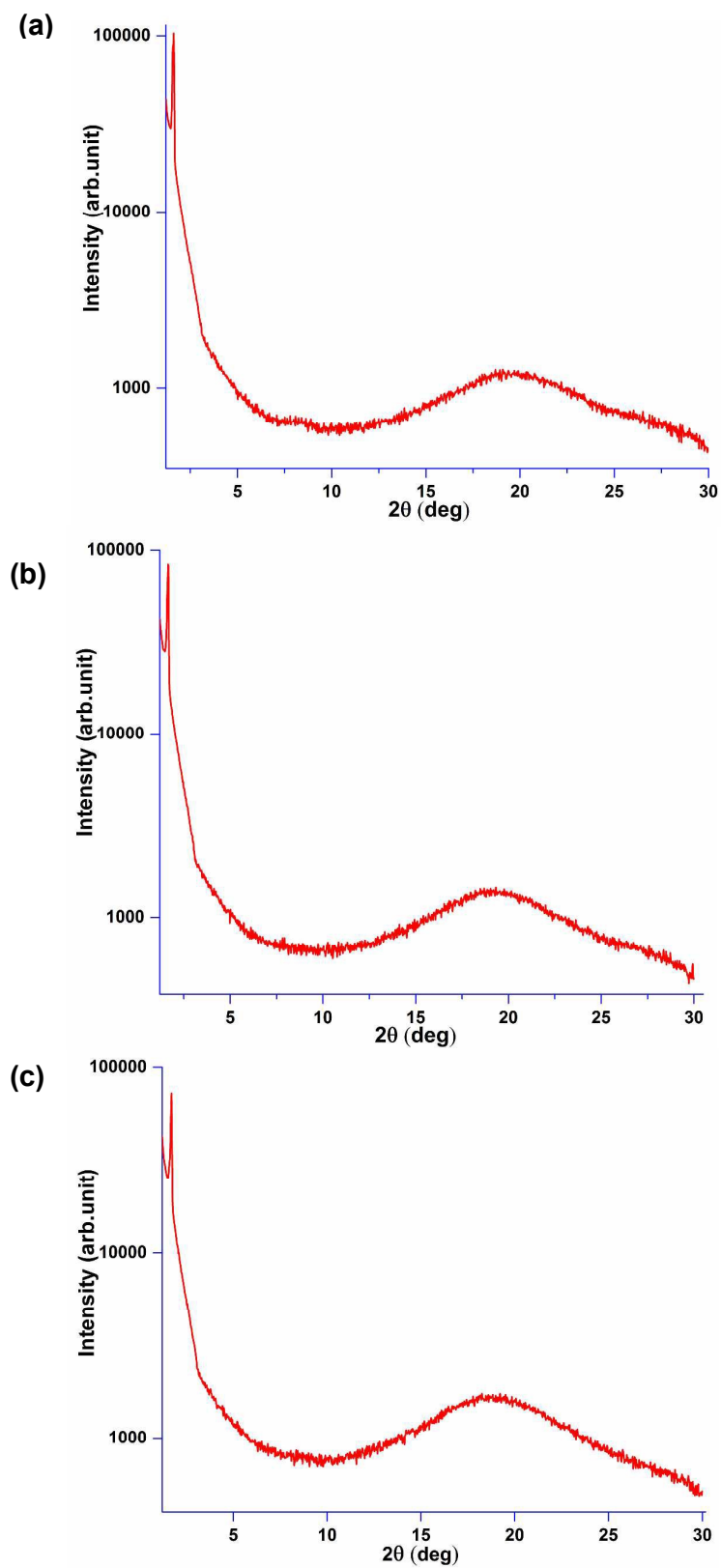


Figure 5

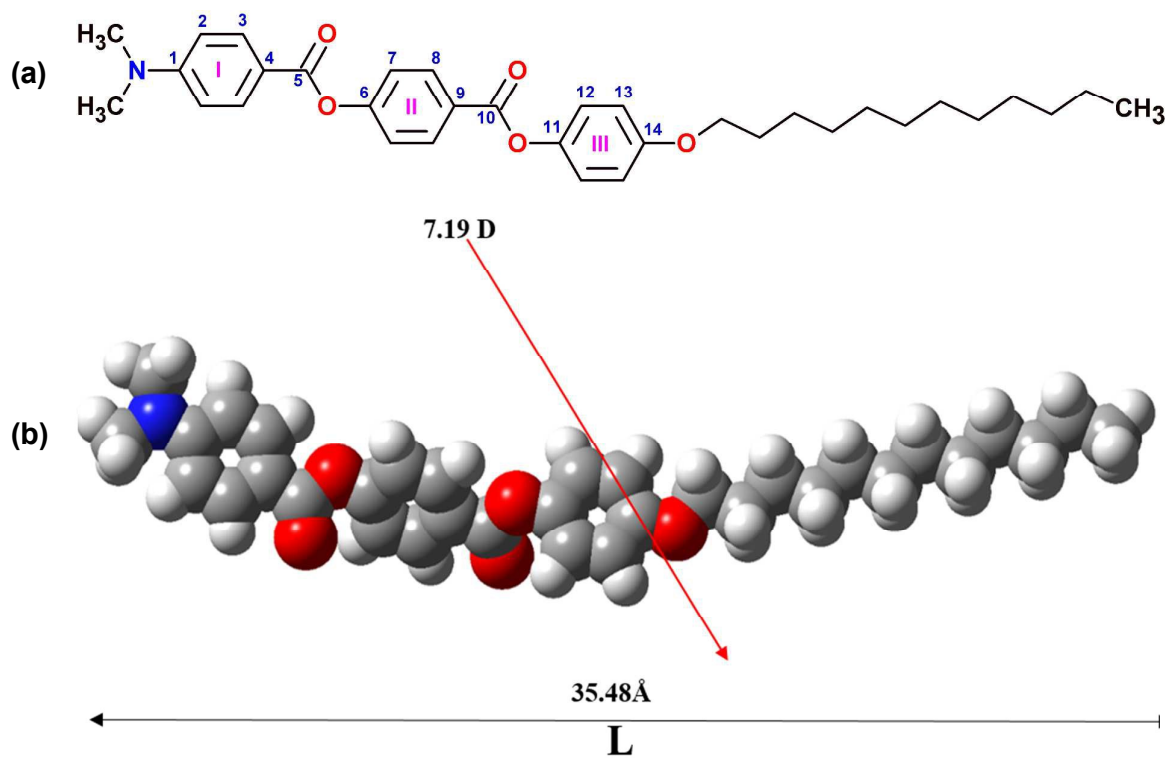


Figure 6

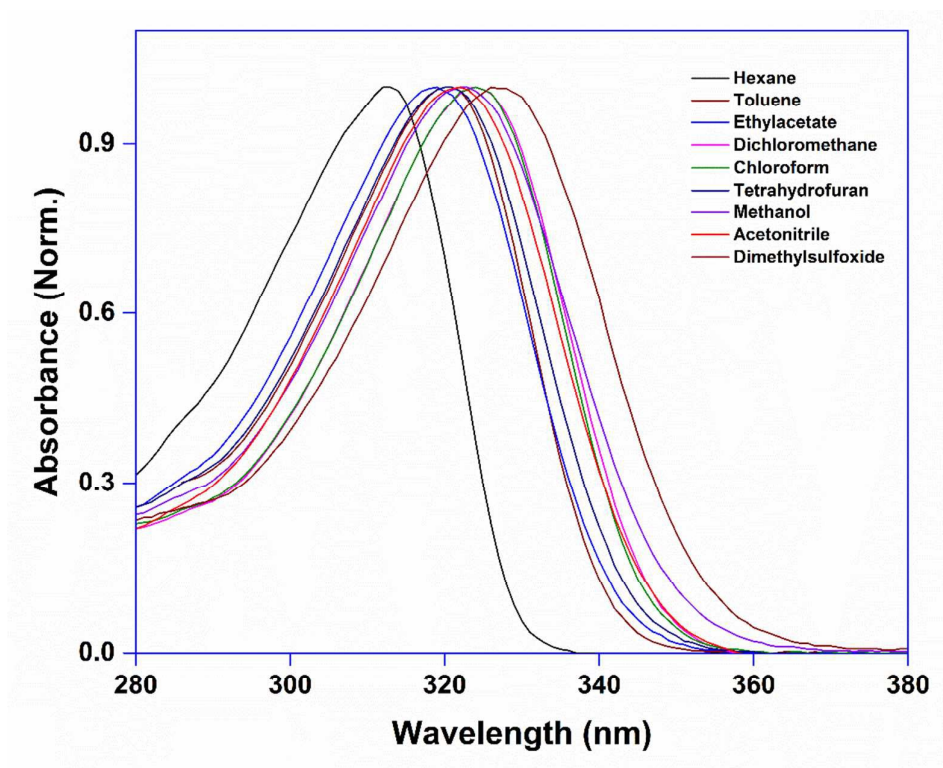


Figure 7

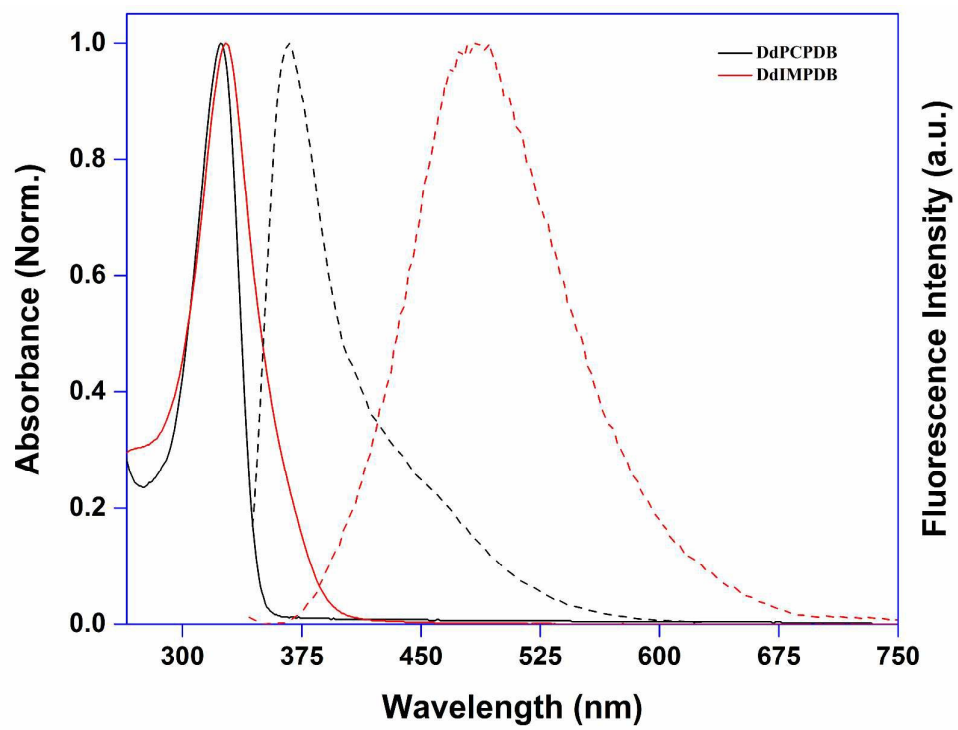


Figure 8

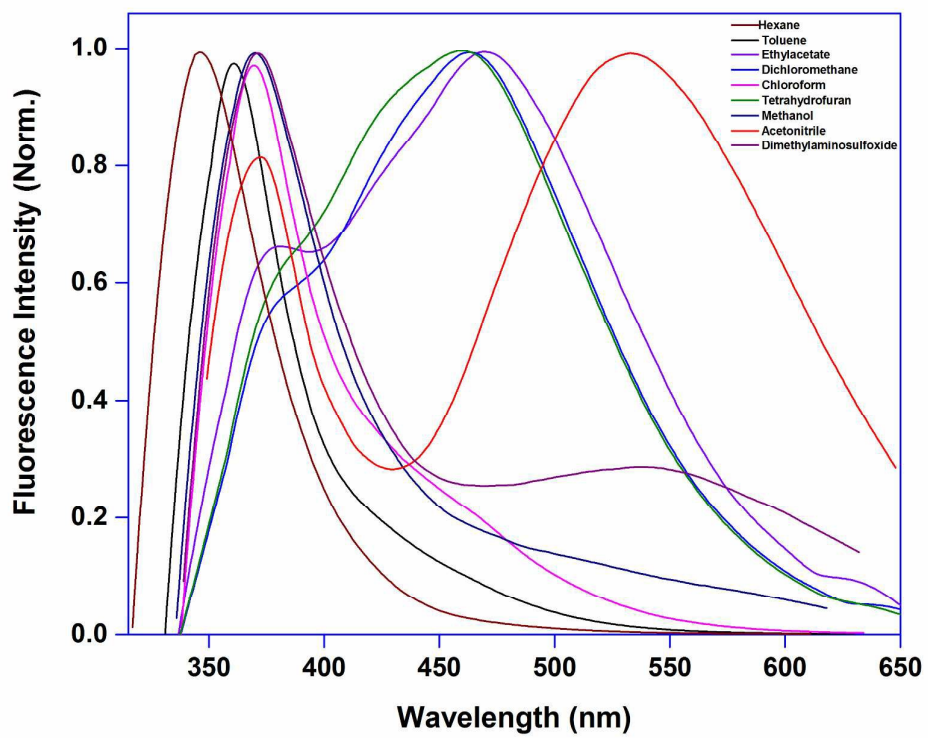


Figure 9

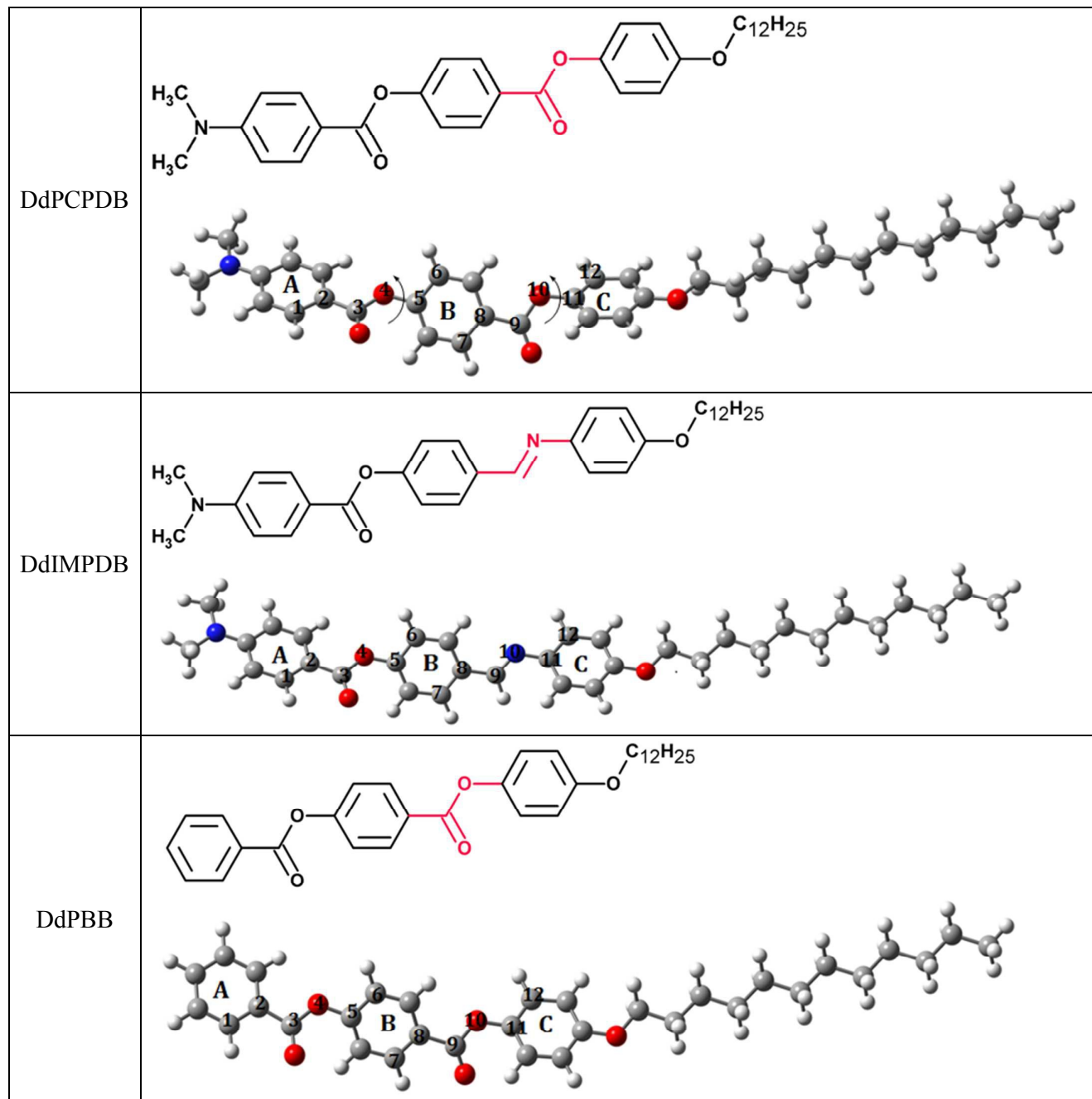


Figure 10

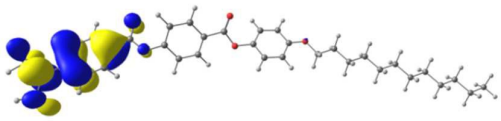
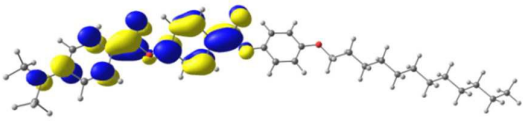
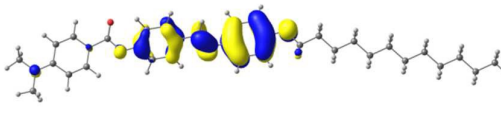
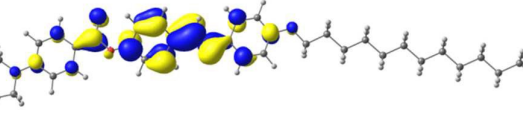
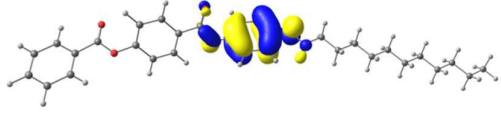
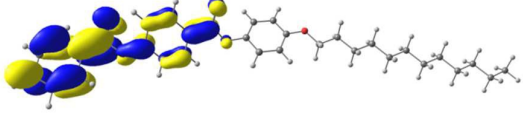
Compounds	HOMO	LUMO
DdPCPDB		
DdIMPDB		
DdPBB		

Figure 11

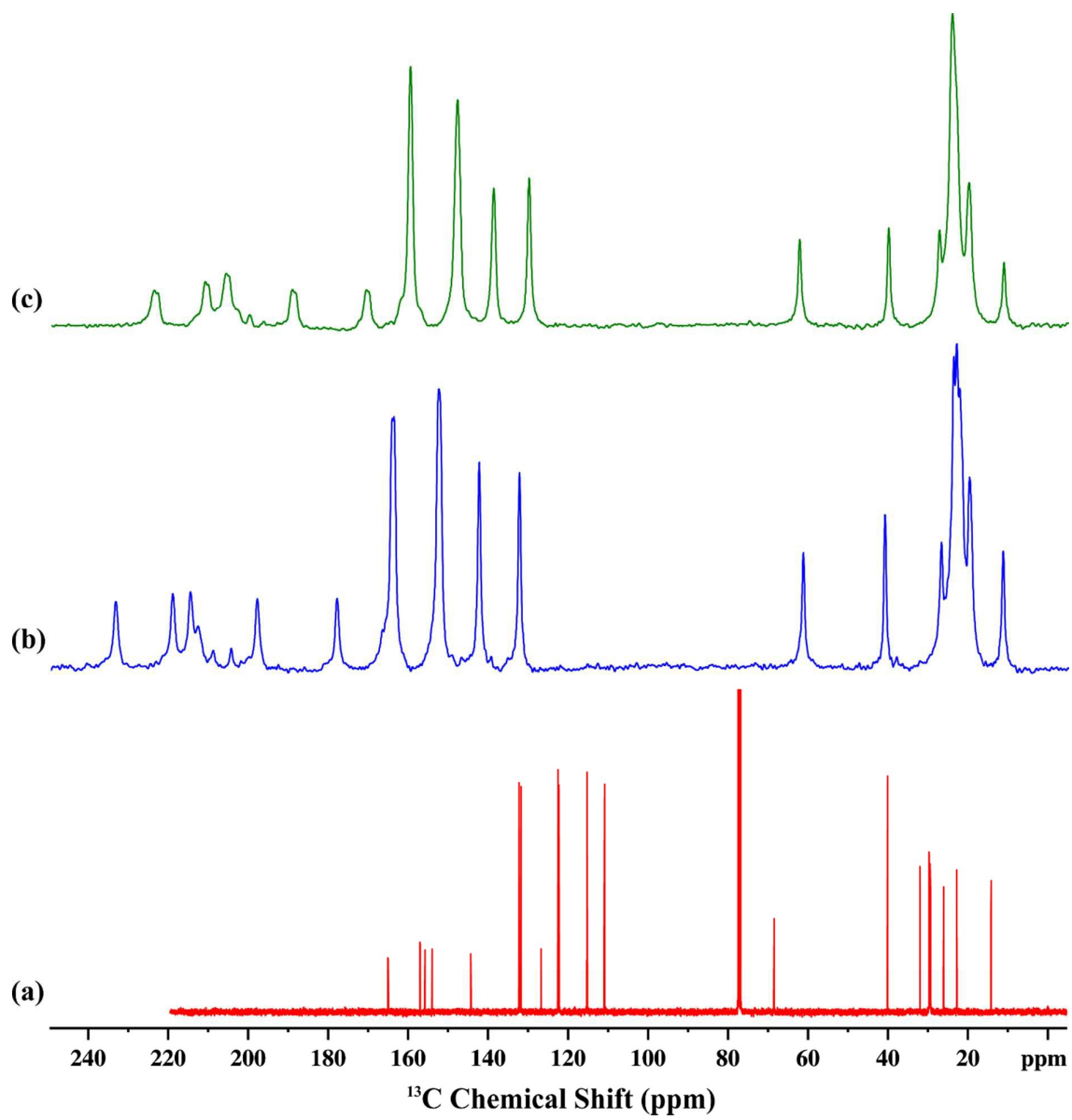


Figure 12

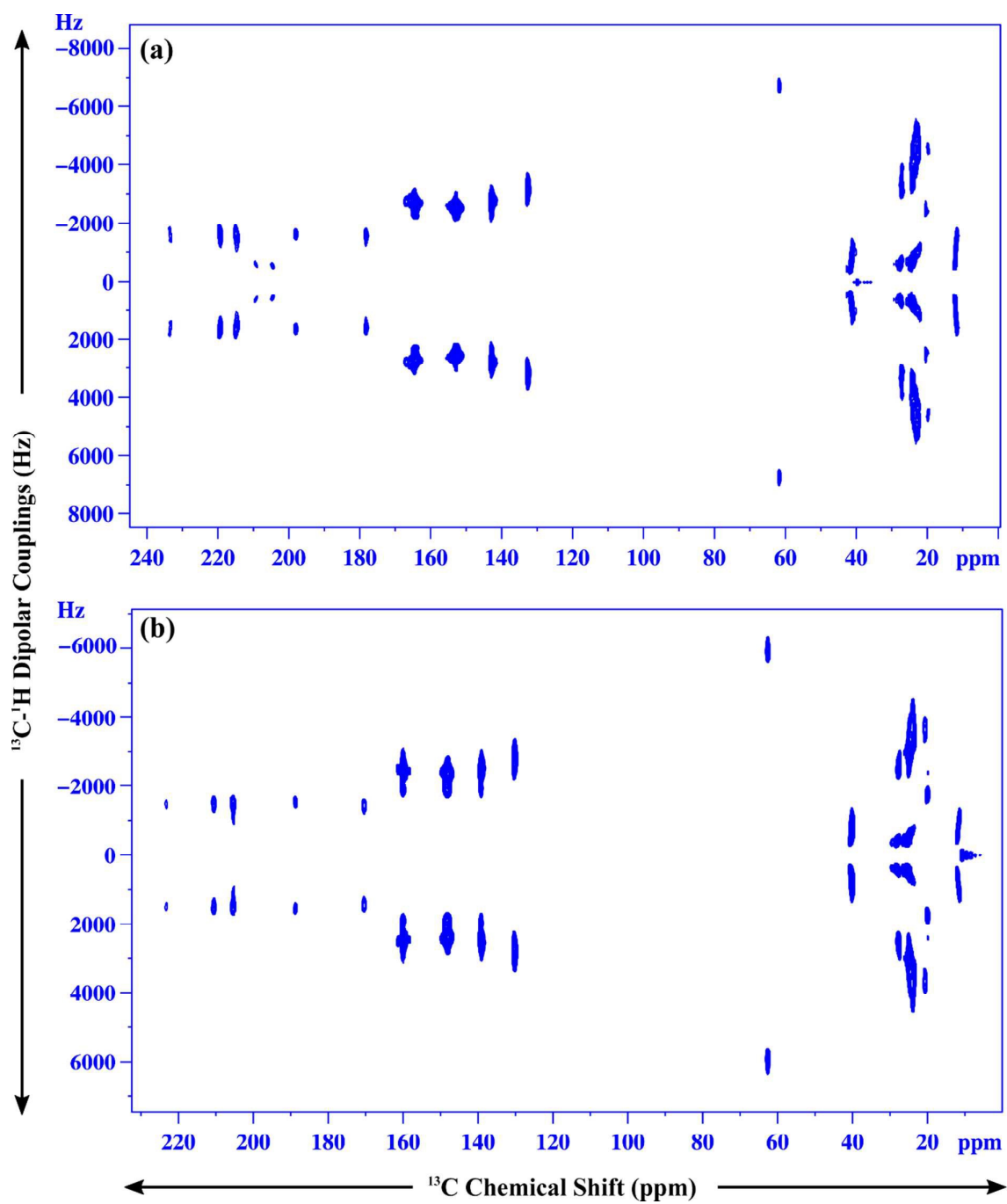
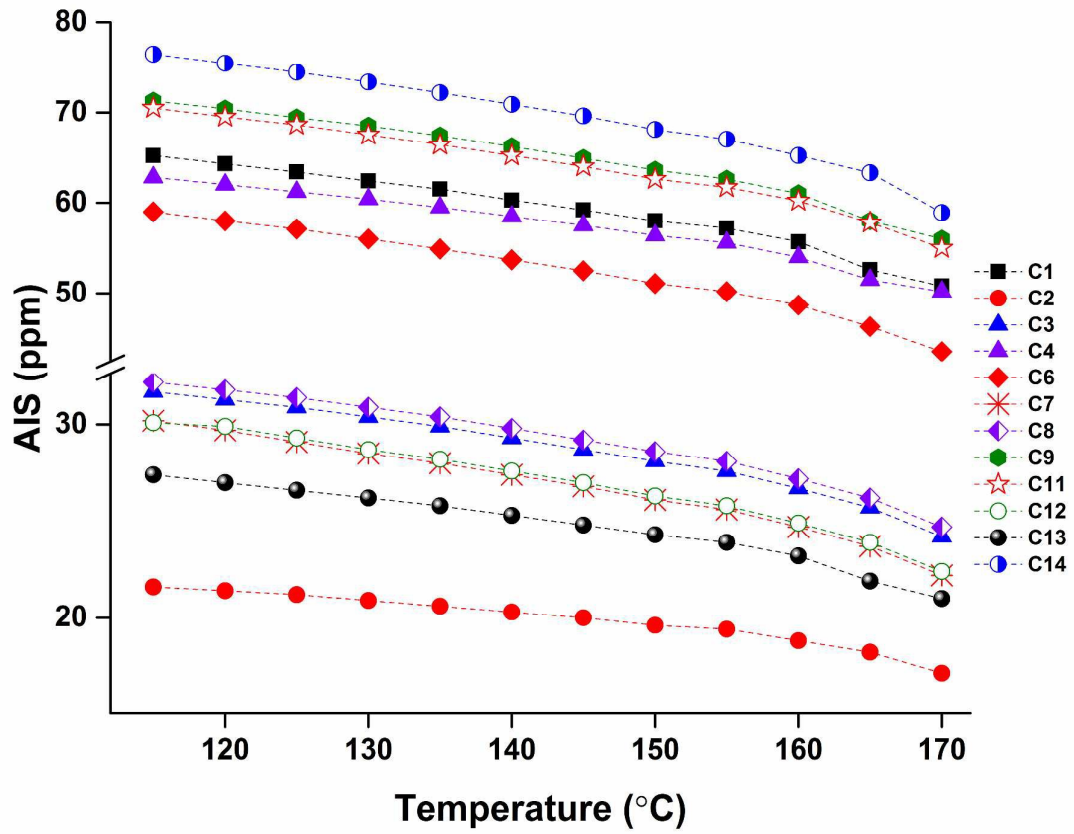
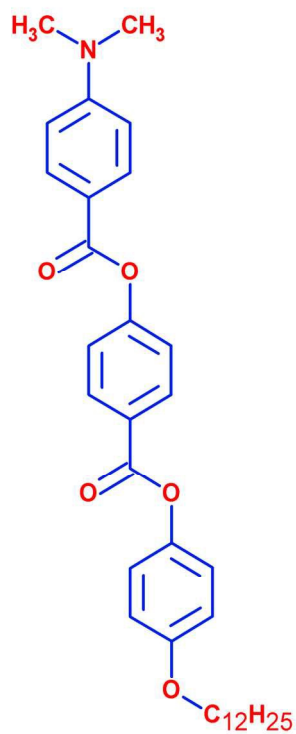
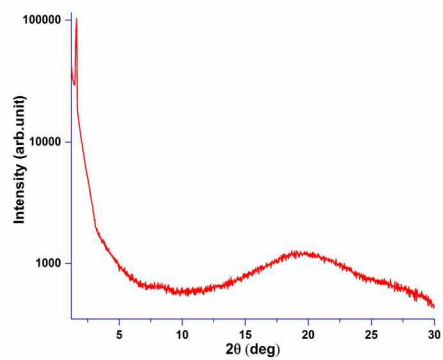


Figure 13

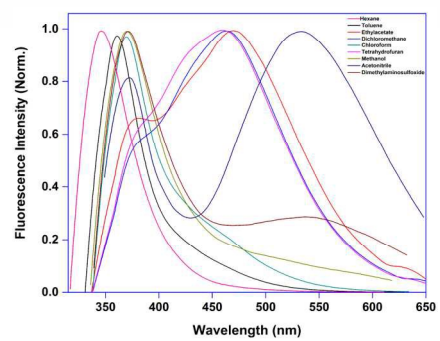




XRD



Fluorescence



^{13}C NMR

